2008 IEEE International Conference on
Robotics and Automation
Pasadena, CA, USA, May 19-23, 2008

Torque Transmission Mechanism with Nonlinear Passive Stiffness using Mechanical Singularity

Masafumi Okada and Shintaro Kino
Dept. of Mechanical Sciences and Engineering, Tokyo TECH
2-12-1 Oookayama Meguro-ku Tokyo, 152-8552 JAPAN
okada@mep.titech.ac.jp

Abstract— **To introduce a passive compliant mechanism for robot joints is an effective way for impact absorption. However, because robot joints also require high torque transmission characteristic, the simultaneous implementation of stiffness and softness is a significant issue. In this paper, we develop a torque transmission mechanism with nonlinear passive stiffness that realizes from zero to extremely high stiffness based on mechanical singularity. The analysis of nonlinear stiffness is established and the experimental evaluation is shown. A four-legged robot with the proposed mechanism is designed and the effectiveness of high nonlinearity of the proposed mechanism is shown by simulation.**

keywords *nonlinear passive stiffness, closed kinematic chain, mechanical singularity*

I. Introduction

Robots are normally designed with rigid links for precise task execution. However, in this case, an impact force damages to the robot body and its environments, which causes a breakage of members, failure of control system and hurt of people. From flexibility and safety points of view, to introduce softness to robot members or joints gives an effective solution. A soft mechanism is applied for a parts assembly task in a factory [1]. Because an elastic link can yield large power using accumulated potential energy, it is applied for a golf swing robot [2].

For realization of a soft robot, (1) active compliance, (2) passive compliance, and (3) programmable passive compliance are proposed so far. Active compliance is realized by a force control of actuators, and some methods have been reported [3], [4], [5], [6], [7]. However, the active compliance does not completely realize softness in high frequency (for impact force), because of the low frequency response of actuators and/or sensors in the closed loop. Some mechanisms that realize programmable passive compliance with nonlinear spring and additional actuator [8], [9], [10] or with antagonistic wire driven mechanisms [11] have been proposed. These are not simple realization because the additional actuator increases the weight and volume of the robot. The backlash clutch in [12] realizes zero-stiffness and high torque transmission based on mechanical backlash and its control.

Passive compliance is simple and effective for softness of the robots. Because high stiffness for precise task execution would be needed at low link actuation, which is not realized in the conventional softness, the simultaneous realization of stiffness and softness is an important issue, and highly nonlinear stiffness will be effective.

In this paper, we develop a nonlinear passive stiffness mechanism. This mechanism realizes

- zero-stiffness based on mechanical singularity
- high nonlinearity of stiffness

A four-legged robot with the proposed mechanism is designed and the effectiveness of high nonlinearity of the proposed mechanism is shown by simulation.

II. Zero-stiffness based on mechanical singularity

A. Mechanism

Joints and links configuration of the proposed mechanism is shown in figure 1. The rotational axes of joints $R_1 \sim R_5$ are

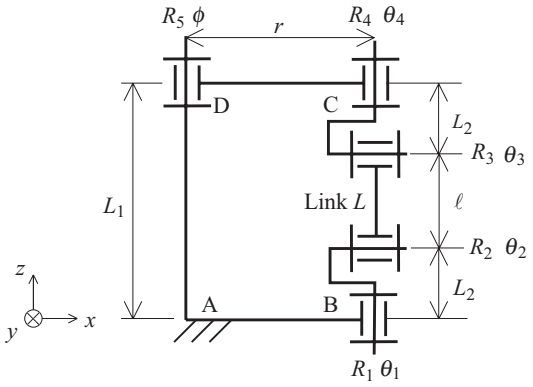

Fig. 1. Joints and links configuration of the proposed mechanism

set along z-axis, x-axis, x-axis, z-axis and z-axis respectively. Their rotation angles are defined by $\theta_1 \sim \theta_4$ and ϕ. Figure 2 shows the cross-section drawing of the prototype. The input torque τ_{in} that works Disk D_{in} is transmitted to τ_{out} on Disk D_{out} through Link L. Roller bearings are used for R_2 and R_3, ball bearings are used for other joints. To reduce the influence of backlash, pre-tension is added to link L by tightening the screw in S. In the following of this section, all materials are assumed to be rigid.

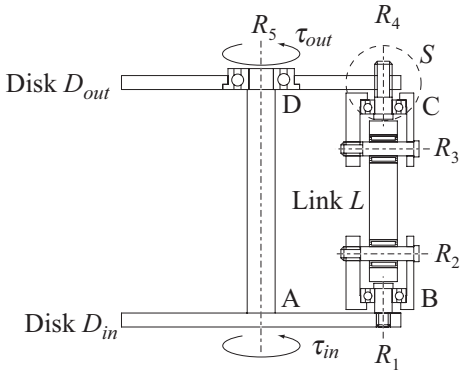

Fig. 2. Cross-section view of the proposed mechanism

B. Zero-stiffness analysis based on null space of Jacobian matrix of constraints

In general, the degree-of-freedom (DOF) F of a 3D mechanism is calculated by

$$F = 6(n-1) - \sum_i (6-i)n_i \tag{1}$$

where n means the number of links and n_i means the summation of i-DOF revolute pairs. The DOF of the proposed mechanism F_p is calculated by $F_p = -1$ ($n = 5$, $n_1 = 5$). Because $\ell = L_1 - 2L_2$ yields the dependency of the constraints, $F_p = 0$ is obtained, which means this mechanism is a structure and it does not move from mechanical DOF point of view.

On the other hand, by considering the closed loop of A→ B→ C→ D→ A, the following constraints of this mechanism are satisfied.

$$\begin{bmatrix} f^T(\theta_1,\theta_2,\theta_3,\theta_4,\phi) & 1 \end{bmatrix}^T = L_x^r L_z^{L_2} R_z^{\theta_1} R_x^{\theta_2} L_z^{\ell} R_x^{\theta_3} R_z^{\theta_4} L_z^{L_2} L_x^{-r} R_z^{\phi} L_z^{-L_1} e_0 = e_0 \tag{2}$$

$$e_0 = \begin{bmatrix} 0 & 0 & 0 & 1 \end{bmatrix}^T \tag{3}$$

$$\mathrm{diag}\left\{\begin{bmatrix} g^T(\theta_1,\theta_2,\theta_3,\theta_4,\phi) & 1 \end{bmatrix}\right\} = R_z^{\theta_1} R_x^{\theta_2} R_x^{\theta_3} R_z^{\theta_4} R_z^{\phi} I_4 = I_4 \tag{4}$$

where $I_4 \in R^{4\times4}$ means identity matrix, R_i^j, $L_i^j \in R^{4\times4}$ mean the coordinates transformation of rotation and translation respectively by j on i axis. diag$\{[a_1\ a_2\ \cdots\ ]\}$ means a diagonal matrix whose diagonal elements are a_1, a_2, $\cdots$. f and $g \in R^{3\times1}$ give the position and orientation constraints respectively. There are six independent constraints that are satisfied at

$$\Theta = \begin{bmatrix} \theta_1 & \theta_2 & \theta_3 & \theta_4 & \phi \end{bmatrix}^T = 0 \tag{5}$$

Consider the minimal change $\Delta\theta_i$ and $\Delta\phi$ for θ_i and ϕ. By neglecting more than second order minimal value, f and g are approximated at given Θ_0 as follows.

$$\begin{bmatrix} f(\Theta_0+\Delta\Theta) \\ g(\Theta_0+\Delta\Theta) \end{bmatrix} = \begin{bmatrix} f(\Theta_0) \\ g(\Theta_0) \end{bmatrix} + J(\Theta_0)\Delta\Theta \tag{6}$$

$$\Delta\Theta = \begin{bmatrix} \Delta\theta_1 & \Delta\theta_2 & \Delta\theta_3 & \Delta\theta_4 & \Delta\phi \end{bmatrix}^T \tag{7}$$

$$J(\Theta_0) = \left[\begin{bmatrix} \frac{\partial f(\Theta)}{\partial \Theta} \end{bmatrix}^T \quad \begin{bmatrix} \frac{\partial g(\Theta)}{\partial \Theta} \end{bmatrix}^T \right]^T \Bigg|_{\Theta=\Theta_0} \in R^{6\times5} \tag{8}$$

When the second term of the right-hand side in equation (6) is equal to zero, $\Theta_0 + \Delta\Theta$ also satisfies the constraints as

$$f(\Theta_0+\Delta\Theta) = \begin{bmatrix} 0 & 0 & 0 \end{bmatrix}^T \tag{9}$$

$$g(\Theta_0+\Delta\Theta) = \begin{bmatrix} 1 & 1 & 1 \end{bmatrix}^T \tag{10}$$

which means this mechanism can move to the direction of $\Delta\Theta$ without any strain of members, that is to say, the stiffness of this mechanism is equivalent to zero to the direction of $\Delta\Theta$. When the rank of J is less than 5, non-zero $\Delta\Theta$ exists, which comes from mechanical singularity.

On the proposed mechanism, rank of J at $\Theta_0 = 0$ is calculated as

$$\mathrm{rank}\ J = 3\ (<5) \tag{11}$$

The orthogonal bases of the null-space of J are obtained as

$$\Delta\Theta_1 = \begin{bmatrix} -0.71 & 0 & 0 & 0.71 & 0 \end{bmatrix}^T \tag{12}$$

$$\Delta\Theta_2 = \begin{bmatrix} 0.33 & -0.41 & 0.41 & 0.33 & -0.66 \end{bmatrix}^T \tag{13}$$

$\Delta\Theta_1$ means link L rotates around z axis. On the other hand, $\Delta\Theta_2$ means the upper disk can rotate $\Delta\phi$ because $\Delta\phi \neq 0$, which means this mechanism has zero-stiffness on R_5 axis at $\Theta = 0$ in spite of consisting of rigid links.

III. Stiffness Analysis of the Mechanism

A. Prototype of the proposed mechanism

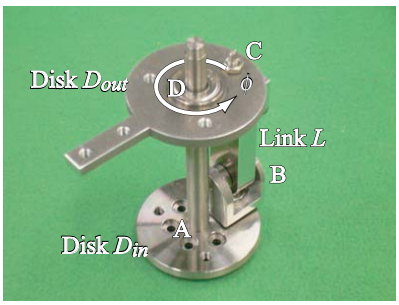

Fig. 3. Prototype of the proposed mechanism

Fig. 4. Twist motion of the designed mechanism

Figure 3 shows the prototype of the proposed mechanism. In this section, it is assumed that link L is elastic and other members are rigid and backlash of the bearings are small. The rotation of D_{out} by ϕ yields nonlinear spring

characteristic because of the elasticity of link L. Figure 4 shows the twist motion of the mechanism. In this figure, there are three links L, which is for high strength.

B. Force and momentum working on L

Force and momentum that apply to L in the twist motion are investigated. Assume that length of link L changes from ℓ to $\ell+\lambda$ due to the rotation by ϕ on R_5 axis as shown in figure 5. Figure 5-(b) shows the top view of figure 5-(a). One straight line passing through points B and C is

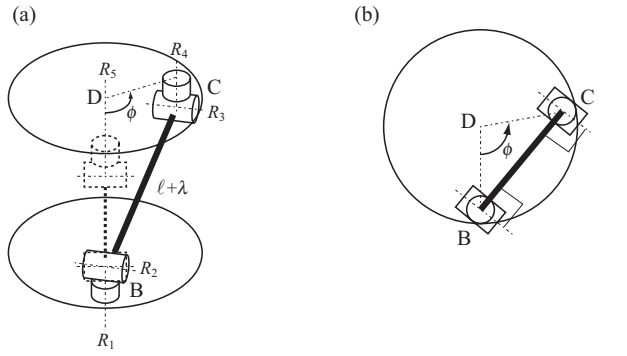

Fig. 5. Relationship between ϕ and $\ell+\lambda$

uniquely decided and R_1, R_4 rotate so that R_2, R_3 axes are orthogonal to this line. The rotation angles are represented by $\theta_1 = -\theta_4 = (\phi-\pi)/2$. This result is derived from two parallelisms of R_1, R_4 axes and R_2, R_3 axes. From these considerations any momentum do not apply, but tension for the length direction applies to link L with respect to the rotation ϕ.

C. Definition of nonlinear stiffness

The torsional stiffness K_ϕ on R_5 axis of this mechanism is calculated. In this paper, nonlinear stiffness is defined from the following consideration. The torque τ that arises according to the rotation ϕ is represented by $\tau = \tau(\phi)$. Consider a

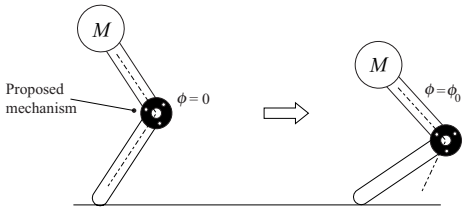

Fig. 6. Link mechanism with the proposed mechanism

two-link mechanism with the proposed mechanism as shown in figure 6. Because of the mass M, the proposed mechanism rotates $\phi = \phi_0$. The generated torque is calculated by

$$\tau_0 = \tau(\phi_0) \tag{14}$$

Let us consider stiffness at $\phi = \phi_0$ in proximity. From equation (14), we obtain

$$\tau_0 + \Delta\tau = \tau(\phi_0) + \left.\frac{d\tau(\phi)}{d\phi}\right|_{\phi=\phi_0} \Delta\phi \tag{15}$$

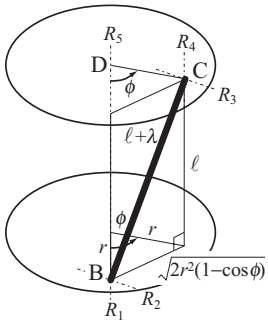

Fig. 7. Relationship between r, ϕ and $\ell+\lambda$

and stiffness K_ϕ at $\phi = \phi_0$ is defined as

$$K_\phi(\phi_0) = \left.\frac{d\tau(\phi)}{d\phi}\right|_{\phi=\phi_0} \tag{16}$$

D. Calculation of stiffness

Let me assume that the spring constant of link L for length direction is defined by K_L (to be a linear spring) and that torsional torque τ on R_5 axis yields rotation by ϕ and the length of link L is changed from ℓ to $\ell+\lambda$. The accumulated kinetic energy E is represented by

$$E = \int_0^\phi \tau(\phi)\ d\phi = \int_0^\lambda K_L\lambda\ d\lambda = \frac{1}{2}K_L\lambda^2 \tag{17}$$

The differential of E with respect to ϕ gives torque τ as following:

$$\frac{dE}{d\phi} = \tau(\phi) = K_L\lambda\frac{d\lambda}{d\phi} \tag{18}$$

The geometry shown in figure 7 gives

$$2r^2(1-\cos\phi) + \ell^2 = (\ell+\lambda)^2 \tag{19}$$

by cosine formula and Pythagorean theorem, and λ is represented by

$$\lambda = \sqrt{2r^2(1-\cos\phi)+\ell^2} - \ell \tag{20}$$

The differential of λ with respect to ϕ gives

$$\frac{d\lambda}{d\phi} = \frac{r^2\sin\phi}{\sqrt{2r^2(1-\cos\phi)+\ell^2}} \tag{21}$$

Equations (18), (20) and (21) lead the torque τ with respect to the function of ϕ as following:

$$\tau(\phi) = K_L\left(r^2\sin\phi - \frac{\ell r^2\sin\phi}{L_\phi(\phi)}\right) \tag{22}$$

$$L_\phi(\phi) = \sqrt{2r^2(1-\cos\phi)+\ell^2} \tag{23}$$

Stiffness K_ϕ is obtained from the differential of equation (22) with respect to ϕ as following:

$$K_\phi(\phi) = K_L\left(r^2\cos\phi - \frac{\ell r^2\cos\phi}{L_\phi(\phi)} + \frac{\ell r^4\sin^2\phi}{L_\phi^3(\phi)}\right) \tag{24}$$

The change of K_ϕ is shown in figure 8. The horizontal axis shows ϕ ($0^\circ\sim8^\circ$) because the deflection cannot be much

because of Yield Point of link L. Link L is assumed to be an 8mm×16mm square pole (material : A2017 aluminum alloy) with length 30mm, $r = 16$mm and $K_L = 1.1 \times 10^8$N/m. In the

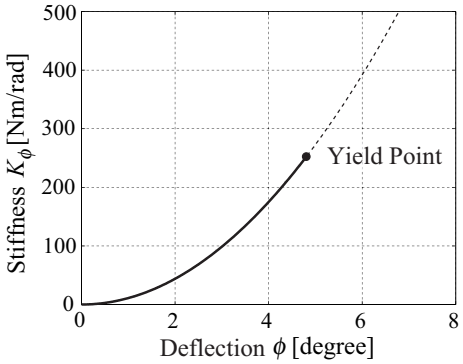

Fig. 8. Stiffness of the mechanism

Yield Point of link L (with 0.1% strain), ϕ is 4.81° and K_ϕ is 256Nm/rad, which is equivalent to the torsional stiffness of duralumin cylinder with 7.5mm diameter and 30mm length. This figure shows that stiffness of this mechanism has zero stiffness at $\phi = 0$ and high nonlinearity acceding to the change of ϕ.

The efficiency of pre-tension T for link L is discussed in the following. Equation (22) is changed by the pre-tension T as following:

$$\tau(\phi) = K_L \left(r^2 \sin\phi - \frac{\ell r^2 \sin\phi}{L_\phi(\phi)} \right) + T \frac{r^2 \sin\phi}{L_\phi(\phi)} \tag{25}$$

The stiffness that is the differential of τ with respect to ϕ is represented by

$$K_\phi(\phi) = K_L \left(r^2 \cos\phi - \frac{\ell r^2 \cos\phi}{L_\phi(\phi)} + \frac{\ell r^4 \sin^2\phi}{L_\phi^3(\phi)} \right) + T \left(\frac{r^2 \cos\phi}{L_\phi(\phi)} - \frac{r^4 \sin^2\phi}{L_\phi^3(\phi)} \right) \tag{26}$$

Because of the influence of T, K_ϕ at $\phi = 0$ becomes

$$K_\phi(0) = \frac{Tr^2}{\ell} \tag{27}$$

that is not zero. The pre-tension T enables the adjustment of the stiffness at $\phi = 0$.

E. Experimental evaluation of nonlinear stiffness

The stiffness of the designed mechanism is measured by experiments. A torque-load by a weight (0.010∼4.0kg) is applied to this mechanism and the rotation angle ϕ is measured with the pre-tension $T = 0$. Two types of the link L as shown in figure 9 are designed. One is a normal link without slits, another is a spring link with slits. The results are shown in figure 10. The relationship between torque τ and rotation angle ϕ has high nonlinearity.

Stiffness of the mechanism with each link is calculated. The results are shown in figure 11. The theoretical values are

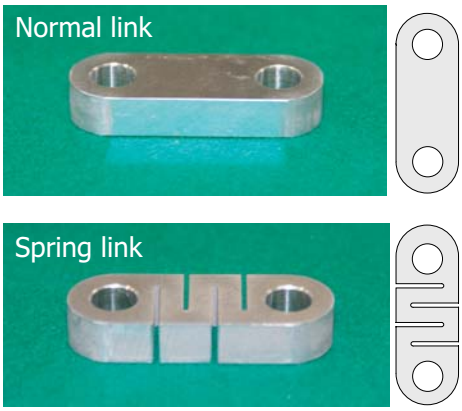

Fig. 9. Two types of designed link L

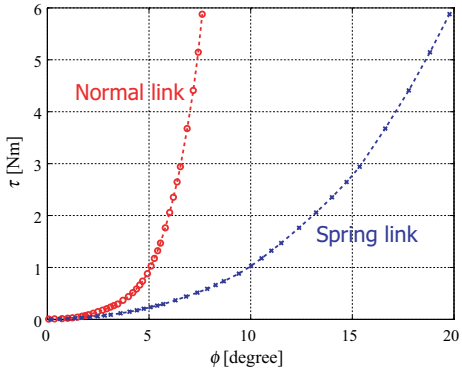

Fig. 10. Torque τ and rotation angle ϕ

shown together. The spring constant of each link is obtained from Finite Element Method (FEM). In both results, the experimental results show lower stiffness than the theoretical values, which is because the strains are caused also in the parts other than link L and backlash of the bearings are not small. These results show the zero-stiffness at $\phi = 0$ and high nonlinearity of the stiffness according to the change of ϕ. The linear stiffness draws a horizontal line (spring constant).

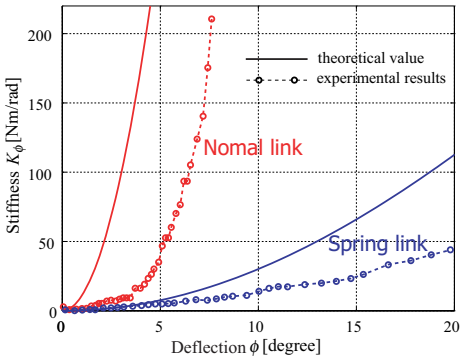

Fig. 11. Stiffness of normal and spring link

IV. Evaluation of the Effectiveness of High Nonlinear Stiffness

A. Four-legged robot

A four-legged robot with the proposed mechanism on the knee joint is designed. Figure 12 shows the photograph of the designed robot and knee joint with the proposed mechanism. The proposed mechanism is indicated by a circle. This mechanism is a compact design of the first prototype shown in figure 3. Each leg has three degrees of freedom. Two DOF are on the base (z-axis and x-axis) and one is on the knee (x-axis). 60W DC motor and 1:50 reduction gear are used for each joint. The size of this robot is about 350mm(width)×450mm(length)×450mm(height) and the weight is about 15kg. The four-legged robot requires:

- High stiffness to support the body weight and to yield high power for motion
- High softness to absorb the impact force

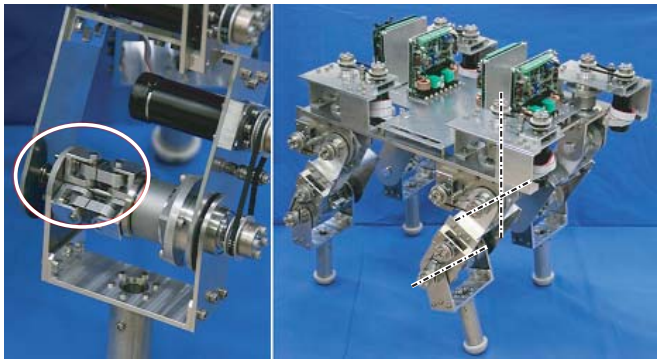

Fig. 12. Four-legged robot with the proposed mechanics

B. Body weight support

To evaluate the effectiveness of nonlinear stiffness of the proposed mechanism, the robot body motion on landing is calculated. As shown in figure 13, the robot falls form the

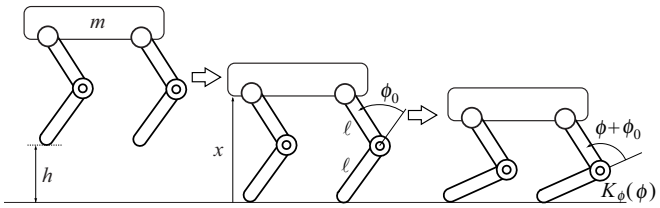

Fig. 13. Robot motion on landing

height h and lands bending its knee joints, which yields the torque by the stiffness to support the body. The motion of the body height x is shown in figure 14. We set $h = 0.1$m, the length of the legs $\ell = 0.2$m and $m =$ 10, 20 and 30kg. The solid lines show the results with the proposed mechanism (nonlinear spring) on the knee joint. For comparison, the dashed lines show the results when a linear torsional spring is used. The spring constant of the linear spring is set so as

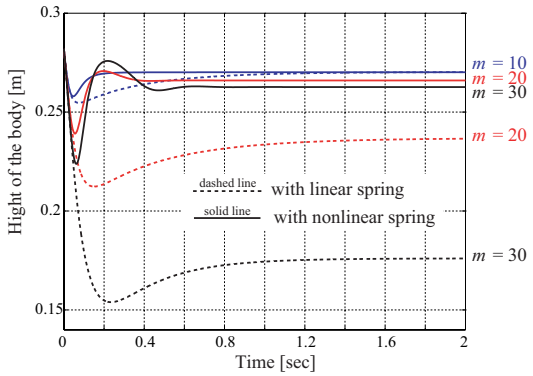

Fig. 14. Body motion on the four-legged robot

to the final value of x with linear spring be equal to that of nonlinear spring when m = 10. The damping parameter of the knee joint is selected appropriately. Figure 15 shows the

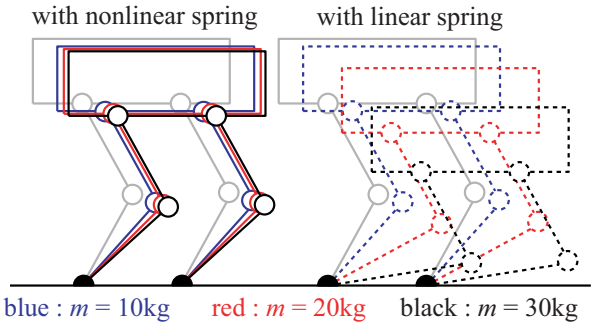

Fig. 15. Final position of the robot

final positions of the robot. These results show that, when we use a linear spring, the final value of x changes in proportion to weight m. On the other hand, when the nonlinear spring is used, the final value of x has small change, which means high stiffness to support the robot body is realized.

C. Impact force absorption

Let me consider the applied force that is caused by the collision with an obstacle as shown in figure 16. The

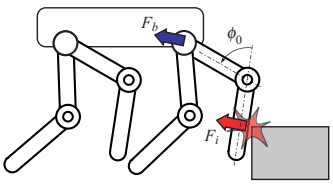

Fig. 16. Collision with an obstacle

impulsive force F_i applies to leg and it is transferred to the body by F_b. To investigate the impact force, we obtain the frequency response form F_i to F_b by using the input

$$F_i = A\sin(\omega t) \tag{28}$$

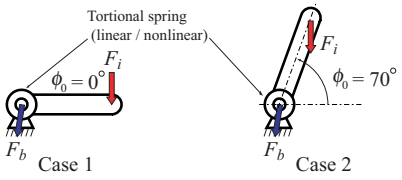

Fig. 17. Model for frequency responses

based on two models shown in figure 17. By the curve fitting method, the transfer function

$$F_b = G(s)F_i \tag{29}$$

is obtained. Frequency response depends on the input amplitude because of high nonlinearity, and A is set 10 and 100. The results are shown in figure 18. These figures show that

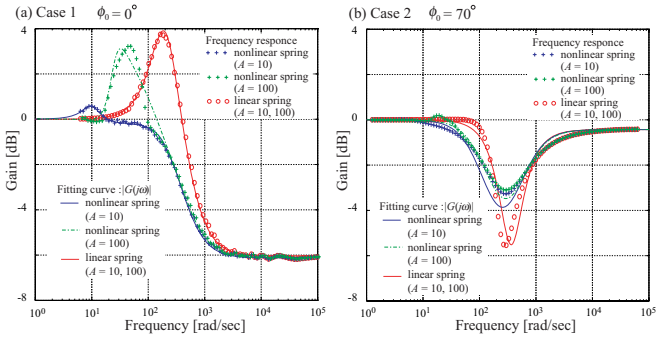

Fig. 18. Frequency responses

the impact force dose no become smaller even if we use the nonlinear spring (zero stiffness at $\phi = 0$) because the initial value of the impulse response is obtained from the following Initial value theorem.

$$F_b(0) = \lim_{s\to\infty} sG(s) = \infty \tag{30}$$

Based on the obtained transfer function, the impulse $P(t)$

$$P(t) = \int_0^t F_b(t)dt \tag{31}$$

is calculated. The results are shown in figure 19. These values are obtained from the step responses of $G(s)$. These figures

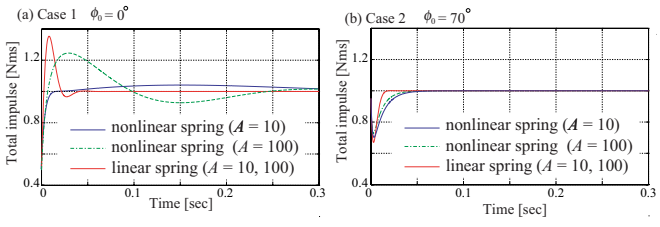

Fig. 19. Total impulse of the collision with an obstacle

show that the total impulse will be smaller when nonlinear spring is utilized.

V. Conclusions

In this paper, we develop a torque transmission mechanism with nonlinear passive stiffness. The results of this paper are as follows:

- Based on mechanical singularity of the closed kinematic chain, zero-stiffness is realized.
- Zero-stiffness and nonlinear stiffness of the proposed mechanism are analyzed based on the kinematic constraints and they are evaluated by the experiments.
- A four-legged robot is designed with the proposed mechanism on knee joint.
- The effectiveness of high nonlinear stiffness of the proposed mechanism for supporting the body and impact absorption is shown by simulations.

Acknowledgment

This research is supported by the "Motion emergence and mutual progression of robot body and intelligence from the dynamical point of view" under Grants-in-Aid for Scientific Research (Category Encouragement of Young Scientists (A)) of Japan Society for the Promotion of Science.

References

[1] Y. Xu and R. P. Paul, "A robot compliant wrist system for automated assembly," in *Proc. of IEEE International Conference on Robotics and Automation (ICRA'90)*, vol. 3, 1990, pp. 1750–1755.

[2] C. Xu, T. Nagaoka, A. Ming, and M. Shimojo, "Motion control of golf swing robot based on target dynamics," in *Proc. of the 2006 IEEE/RSJ International Conference on Intelligent Robots and Systems (IROS'06)*, 2006, pp. 2524–2550.

[3] R. P. C. Paul and B. Shimano, "Compliance and control," in *Proc. of the 1976 Joint Automatic Control Conference*, 1976, pp. 694–699.

[4] H. Hanafusa and H. Asada, "Stable pretension by a robot hand with elastic fingers," in *Proc. of the 7th International Symposium on Industrial Robots*, 1978, pp. 361–368.

[5] N. Hogan, "Mechanical impedance control in assistive devices and manipulators," in *Proc. of the 1980 Joint Automatic Control Conference*, 1980, pp. TA10–B.

[6] J. K. Salisbury, "Active stiffness control of a manipulator in cartesian coordinates," in *Proc. of the IEEE Conference on Decision and Control*, 1980.

[7] N. Hogan, "Impedance control: An approach to manipulation: Part 1-3."

[8] K. F. L-Kovitz, J. E. Colgate, and S. D. R. Carnes, "Design of components for programmable passive impedance," in *Proc. of IEEE International Conference on Robotics and Automation*, 1991, pp. 1476–1481.

[9] T. Morita, N. Tomita, T. Ueda, and S. Sugano, "Development of force-controlled robot arm using mechanical impedance adjuster," in *Proc. of IEEE International Conference on Intelligent Robots and Systems*, 1999, pp. 1216–1221.

[10] M. Okada, Y. Nakamura, and S. Ban, "Design of programmable passive compliance shoulder mechanism," in *Proc. of IEEE International Conference on Robotics and Automation*, 2001, pp. 348–353.

[11] J. Yamaguchi, D. Nishino, and A. Takanishi, "Realization of dynamic biped walking varying joint stiffness using antagonistic driven joints," in *Proc. of the 1998 IEEE International Conference on Robotics and Automation*, 1998, pp. 2022–2029.

[12] M. Okada, T. Shinohara, T. Gotoh, S. Ban, and Y. Nakamura, "Double spherical joint and backlash clutch for lower limbs of humanoids," in *Proc. of IEEE International Conference on Robotics and Automation*, 2003, pp. 491–496.